

# Parallel HOP: A Scalable Halo Finder for Massive Cosmological Data Sets

Stephen Skory, Matthew J. Turk, Michael L. Norman, and Alison L. Coil

*Center for Astrophysics and Space Sciences,  
University of California, San Diego, CA 92093*

{sskory, mjturk, mlnorman, acoil}@ucsd.edu

## ABSTRACT

Modern N-body cosmological simulations contain billions ( $10^9$ ) of dark matter particles. These simulations require hundreds to thousands of gigabytes of memory, and employ hundreds to tens of thousands of processing cores on many compute nodes. In order to study the distribution of dark matter in a cosmological simulation, the dark matter halos must be identified using a halo finder, which establishes the halo membership of every particle in the simulation. The resources required for halo finding are similar to the requirements for the simulation itself. In particular, simulations have become too extensive to use commonly-employed halo finders, such that the computational requirements to identify halos must now be spread across multiple nodes and cores. Here we present a scalable-parallel halo finding method called Parallel HOP for large-scale cosmological simulation data. Based on the halo finder HOP, it utilizes MPI and domain decomposition to distribute the halo finding workload across multiple compute nodes, enabling analysis of much larger datasets than is possible with the strictly serial or previous parallel implementations of HOP. We provide a reference implementation of this method as a part of the toolkit yt, an analysis toolkit for Adaptive Mesh Refinement (AMR) data that includes complementary analysis modules. Additionally, we discuss a suite of benchmarks that demonstrate that this method scales well up to several hundred tasks and datasets in excess of  $2000^3$  particles. The Parallel HOP method and our implementation can be readily applied to any kind of N-body simulation data and is therefore widely applicable.

*Subject headings:* galaxies: halos — methods: data analysis — methods: N-body simulations

## 1. Introduction

The overarching goal of a cosmological N-body simulation is to accurately model the hierarchical distribution of matter that is observed in the universe. It is computationally efficient to model the mass distribution with collisionless massive particles that represent dark matter. The first step in analyzing the distribution of dark matter in a simulation is to locate the dark matter halos, which are collapsed over-dense regions that host galaxies. Finding haloes is a computationally difficult task that requires establishing the halo memberships of all the particles in a simulation. Similarly to the N-body simulation itself, it is impractical to compare every pair of particles when doing calculations and approximations must be made for the sake of efficiency.

The field of halo finders for simulated cosmological data is well-populated. All are compromises between physical accuracy and computational speed. On one end of the spectrum is the Friends-of-Friends (FOF) halo finder (Davis et al. 1985), which is simple and computationally fast. FOF builds halos by linking together all particles that are closer than a certain distance from each other. Most particles will have several linkages, and by recursively following links between particles, a halo can be identified from the set of inter-linked particles. However, FOF does not use any physical property of the halo during selection and is well known to over-connect halos by filamentary bridges (Eisenstein and Hut 1998). In the same article, Eisenstein and Hut present a method called HOP that improves halo finding by considering the physical density of each particle rather than just locality. The density of each particle is found by using a smoothing kernel over the neighboring particles, and halos are built up by recursively linking particles to their densest nearest neighbor, forming long chains of particles. These chains are then merged to form the final halos. Halos identified by HOP are far less filamentary than those of FOF, and are more likely to be physically meaningful. However, HOP does not consider gravitational boundedness (kinetic plus potential energy) when assembling halos. At higher computational expense, DENMAX (Gelb and Bertschinger 1994) and its improvement SKID<sup>1</sup> compute physical density similarly to HOP, and also remove gravitationally unbound particles from halos. VOBOZ (Neyrinck et al. 2005) uses Voronoi diagrams (Voronoi 1908) and Poisson statistics to create halos and eliminate unbound particles.

Many modern halo finders have been designed to identify subhalos within larger host halos, something that HOP (and therefore our parallelization of it) does not do. Subhalos are gravitationally-bound objects that reside within or close to larger host halos, such as satellite galaxies. This is often a multi-step processes, where host halos are first found with a simple

---

<sup>1</sup><http://www-hpcc.astro.washington.edu/tools/skid.html>

method (FOF is a popular choice) and then each separately analyzed in greater detail and at higher computational expense. This is the workflow employed by **SUBFIND** (Springel et al. 2001), **PSB** (Kim and Park 2006) and the method described in Shaw et al. (2007). Many methods identify self-bound substructures similarly to the **DENMAX** recipe such as the **BDM** method of Klypin and Holtzman (1997), the **IsoDen** method of Pftitzner et al. (1997), and the method described in Weller et al. (2005). Halo finders like **6DFOF** (Diemand et al. 2006) and **HSF** (Maciejewski et al. 2009) locate substructure by extending the halo finding into the phase space of the particles. Hierarchical FOF (Klypin et al. 1999) builds a hierarchy of substructure by running FOF over a range of linking lengths. Somewhat similarly, Adaptive FOF (van Kampen 1995) finds substructure by automatically adjusting the linking length based on local density. Hierarchies of substructure can also be found by basing halos on the hierarchy of grids used in an Adaptive Mesh Refinement (AMR) simulation (**MHF** Gill et al. (2004), and its replacement **AHF** Knollmann and Knebe (2009)). An interesting method based on HOP, called **ADAPTAHOP** (Aubert et al. 2004), is capable of locating substructure and offers some ideas for the future direction of Parallel HOP (see §6.1).

All modern cosmological simulation codes are run using the distributed parallel model, in which both the memory and workload are handled by multiple processing units on many discrete networked computing nodes. Increasingly, the simulations produce datasets that can only be analyzed on similarly sized resources to what is required for the simulation itself. In our research we use the Eulerian AMR hydrodynamical and cosmological code **ENZO** (O’Shea et al. 2004; Norman et al. 2007), which is capable of running simulations with billions ( $10^9$ ) of particles that require terabytes of memory. Traditionally, HOP has been distributed with **ENZO** and used as the primary halo finder for **ENZO** data. The publicly available version of HOP<sup>2</sup> (and the version distributed with **ENZO**, which adds a wrapper that can read **ENZO** data) is not capable of analyzing very large datasets because it is not parallel-capable. Even if a shared memory computer could contain the data for billions of particles, the computational time for serially examining that much data would be immense. Parallel halo finders, such as **AHF** and **FOF** (Springel 2005) would be feasible, but changing halo analysis platforms would make direct comparison to previous **ENZO**/HOP results difficult, impeding both resolution studies and simulation verification.

Here we present a parallelized version of HOP, called Parallel HOP. It is an update to the HOP method that can analyze arbitrarily large datasets on as many cores and compute nodes as needed. In Section 2 we describe the original HOP method in detail, as well as the limitations of two previous parallel versions of HOP. The general Parallel HOP method is

---

<sup>2</sup><http://cmb.as.arizona.edu/~eisenste/hop/hop.html>

outlined step-by-step in Section 3, which is applicable to any kind of N-body cosmological data. Our implementation of Parallel HOP is described in Section 4, which is easily adaptable to non-ENZO data. We benchmark our implementation in Section 5, and show that it can analyze very large datasets efficiently, and that it scales well with core count. We discuss future possibilities of improving Parallel HOP in Section 6, as well as continuing work on running it concurrently with an ENZO simulation as an inline halo finder. Appendix A provides a guide to understanding the functional pieces that make up the publicly-available source code of our Parallel HOP implementation.

In this paper, computing ‘cores’ refer to the physical units of a computer that execute mathematical instructions, and ‘tasks’ refer to the executables that run on the cores. It is possible to run multiple tasks per core, but in this paper all benchmarks are run with one task per core. Therefore, ‘cores’ and ‘tasks’ are used somewhat interchangeably, although they mean different things.

## 2. HOP

Building halos with the original HOP algorithm requires four stages. The first stage calculates the density of each particle using a local smoothing kernel based on the distances to and masses of its nearest neighbors. The default number of nearest neighbors used for the smoothing kernel is  $N_{\text{dens}}$  (=65 by default), and the kernel always includes the self-same particle. The density for each particle is normalized with respect to the average density of particles in the simulational volume. Therefore, the average density found using HOP is not the same as the average density of the universe.

The nearest neighbors are found using a  $k$ D-tree (Friedman et al. 1977), which is a space-partitioning data structure that allows nearest neighbors to be found much more efficiently than by brute-force. A brute-force nearest neighbor search requires  $O(N^2)$  inter-particle distance calculations, where  $N$  is the number of particles. A  $k$ D-tree reduces the number of operations to  $O(N \log N)$ , with no loss of accuracy. A  $k$ D-tree is built by recursively subdividing a set of data points (in this case, particle positions) into evenly sized ‘buckets’ that typically contain tens of data points. Each data point is assigned uniquely to a bucket, and the buckets are geometrically associated with one another in a tree-like data structure that is referenced when performing nearest neighbor searches. A  $k$ D-tree search is much faster than brute-force because a nearest neighbor search needs only to compute distances to particles in a few nearby buckets, instead of all the particles in the entire dataset.

The next step in HOP is to link each particle to its densest nearest neighbor, which

is the particle in the set of neighbors with the greatest density. This link may be to the self-same particle if it is the densest particle in its set of neighbors. Long chains of particles are built in the third step by ‘hopping’ from lower to higher density particles, following the links found in the previous step. Chains terminate on a particle that is its own densest nearest neighbor. There is no restriction on the shape of the chains, which means that there is also no restriction on the shape of the final halos. Finally, geometrically adjacent chains are merged into final halos according to merging rules and density threshold cutoffs.

A typical set of cutoff values excludes all particles from halos with densities less than 80 times the average density of particles in the simulation, and requires that all final halos have at least one particle with a density 240 times the average. Changing the cutoff values has the strongest effect on the smallest halos. Raising the cutoff values reduces the number of small halos identified, while lower values identify more small halos at the cost of large halos becoming physically extended and over-linked by filamentary low-density bridges.

Chain merging in HOP attempts to merge density maxima inside of density contours, and is done in five steps. A diagram showing example chains and merging possibilities is shown in Figure 1. First, particles with density below a user-set threshold  $\delta_{\text{outer}}$  ( $=80$  by default, as mentioned above) are excluded from becoming members of any final halo. Second, the particle with maximal density is found for each chain, and if that particle’s density is above a peak density threshold  $\delta_{\text{peak}}$  ( $= 3\delta_{\text{outer}}$  by default), it is considered a proto-halo (but it is still considered a chain for future steps, as well). Third, for all particles in chains, the  $N_{\text{merge}}$  ( $=4$  by default) nearest neighbors are found. If a nearest neighbor particle has different chain assignment from another, the average combined density  $\delta_{\text{link}}$  of the two particles is calculated and added to a lookup table of boundary densities between chains. Note that the inter-chain links can be unidirectional—the particle in chain A that has a particle in its set of  $N_{\text{merge}}$  nearest neighbors in chain B, may not itself be in the  $N_{\text{merge}}$  set of any particle in chain B. Fourth, if two proto-halos have a boundary density  $\delta_{\text{link}} \geq \delta_{\text{saddle}}$  ( $=2.5\delta_{\text{outer}}$  by default), they are merged into a combined proto-halo.

The final step which merges sub- $\delta_{\text{peak}}$  chains to proto-halos is the most subtle. Sub- $\delta_{\text{peak}}$  chains are recursively merged to proto-halos by following the densest boundaries between chains “downhill” from proto-halos. As an example referring to Figure 1, in the situation where  $\delta_{\text{BC}} > \delta_{\text{CD}} \geq (\delta_{\text{AD}}, \delta_{\text{DE}})$ , chain D is linked to proto-halo B although it has no direct link to chain B. This specific situation is unlikely, but it illustrates the recursive nature of the sub- $\delta_{\text{peak}}$  chain merging process. Note that because the boundary densities are established between particles on the fringes of chains, the boundary densities may be unrelated to the peak density values (especially if the link crosses a density contour line). It is important to mention here, because it is used in Parallel HOP, that a proto-halo will always merge

with all neighboring proto-halos with which it shares a boundary density greater than or equal to  $\delta_{\text{saddle}}$ . However, sub- $\delta_{\text{peak}}$  chains merge only with one neighboring chain, the chain it shares the greatest (propagated) boundary density with. Therefore the full, global set of chain-neighbor relationships must be found before sub- $\delta_{\text{peak}}$  chains can be merged. This non-local information requirement is one of the most challenging aspects of the HOP method addressed by Parallel HOP.

The input and runtime parameters of HOP are discussed in more detail in §4.1.

## 2.1. Versions of HOP

The publicly available version of HOP is actually several executables that are run consecutively, by hand. Before execution, the end-user must convert their particle data into the native HOP format. There is a re-packaged version of HOP included with ENZO, called ENZO HOP, that simplifies the process by joining the components of HOP together into one executable, and can read ENZO data files natively. While this enables a straightforward pipeline for ENZO data analysis, ENZO HOP does not improve on HOP in any other way.

HOP is an efficient method for finding halos, but if run serially, the running time for analysis of a large dataset can be prohibitive. For example, in our tests running serial HOP on a dataset with  $512^3$  particles, HOP requires on the order of 10 hours and about 8 gigabytes of shared memory. Extrapolation to a larger datasets shows that the computation time and the memory requirements will become prohibitively large.

There are two previous attempts to address the problems of speed and memory usage of original HOP. OpenMP HOP (§2.2) increases the speed by utilizing multiple processing cores on a single shared memory node, and MPI HOP (§2.3) attempts to address both issues by running on multiple nodes and many cores.

## 2.2. OpenMP HOP

OpenMP<sup>3</sup> is a standardized Application Program Interface (API) that allows a C, C++ or Fortran program to utilize more than one processing core on a Symmetric Multi-Processing (SMP) shared memory node. OpenMP HOP, which is part of the MineBench package (Narayanan et al. 2006; Zambreno et al. 2006), parallelizes the most time and

---

<sup>3</sup><http://openmp.org/>

computationally-intensive parts of HOP. At eight processors they find a speedup of more than five over a single processor run for a range of datasets between approximately  $6 \times 10^5$  and  $4 \times 10^6$  particles (see Figure 1 of Zambreno et al.).

However, this implementation does not address the single node memory limits of HOP because of the SMP requirement of OpenMP. Despite the improvements to computation time, the algorithm is not fundamentally changed, and thus does not address the maximum dataset size.

### 2.3. MPI HOP

Message Passing Interface (MPI<sup>4</sup>), is an API that enables multiple programs (or “tasks”) running on one or more SMP nodes to communicate and coordinate with each other, and operate as a single parallel program. The memory and processing cores available for the full job are the amalgamation of the capabilities of the SMP nodes used. MPI HOP, as implemented by Liu et al. (2003), attempts to address the limitations of the original HOP implementation by using data-parallelism via the MPI API. This is done by replacing the original serial  $k$ D-tree with a distributed and parallel  $k$ D-tree. By design, the distributed  $k$ D-tree very effectively balances the workload and memory usage across the nodes. On a dataset with  $\sim 5 \times 10^5$  particles the speedup of MPI HOP is similar to OpenMP HOP through about 8 processors, but flattens at higher processor counts, and by 64 processors the speedup is about 20 (see Figures 6 & 8 from Liu et al.).

According to the text in Liu et al., both the hopping and final group merging are performed in parallel. A thorough inspection of the MPI HOP source code reveals that this is incorrect. Instead, the entirety of the particle data are collected on one task and the work is done in serial, identically to original HOP. This means that MPI HOP is no more capable of analyzing large datasets than the original or OpenMP versions of HOP.

## 3. Parallel HOP Method

Here we outline each step of the Parallel HOP process in detail. Parallel HOP addresses the main shortcomings of the versions of HOP described above. It distributes both the memory and computational load across as many SMP nodes as required, where the minimum number is set by the memory requirements. This implementation successfully distributes the

---

<sup>4</sup><http://www.mpi-forum.org/>

most computationally costly parts of HOP and allows large datasets to be quickly analyzed.

The key to the Parallel HOP method is the local nature of the computational kernel. As mentioned above, the density of each particle depends only on the distances to and masses of the  $N_{\text{dens}}$  nearest neighbors for that particle. If the representation of a particle in the computational kernel’s memory has its full complement of  $N_{\text{dens}}$  nearest neighbors, its density will be calculated correctly. A corollary of this fact is that if all of the neighbors of a particle also have their full and correct compliment of nearest neighbors, the densest nearest neighbor link will be correct for that particular particle.

Parallel HOP uses MPI communication to distribute the work and memory load of the HOP algorithm across multiple SMP nodes. The method and implementation (see §4) share some similarities to MPI HOP, but there are some key differences. Parallel HOP uses a separate and local  $k$ D-tree on each task, and never copies the entire particle dataset onto a single task. Having separate  $k$ D-trees means that the  $O(N \log N)$  operations required for a nearest neighbor search depends on the number of particles on a task, rather than the entire dataset, which increases overall efficiency.

### 3.1. Step By Step

As a visual aid, please refer to Figure 2 for a diagrammatic flowchart of the steps described below.

The first step of Parallel HOP is to spatially subdivide the data into non-overlapping, space-filling subvolumes. Although the subvolumes are restricted to being rectangular prisms, each may be of different size and shape. This flexibility can be used to evenly distribute the workload across the computational resource, which reduces inefficiencies and speeds up the run time (see §4.1.2). Each MPI task is responsible for exactly one subvolume.

Following the identification and mapping of subvolumes to computational tasks, the particle data in those subvolumes can be read into memory without duplication. In Figure 3 each subvolume has an unique set of particles within its local boundaries.

Next, a global lookup table is created that lists subvolumes (or, equivalently tasks) that are geometric neighbors. Subvolumes may be neighbors via direct or periodic face, edge or corner contact. The global lookup table of neighbors, and other lookup tables used below, are a quick-search data object with [key, data] pairs, where the key is an unique identifier (such as MPI task ID or chain label) and the data are values assigned to that particular key. In Figure 3, the global lookup table of subvolume neighbors links subvolumes A and B



together because they share a face boundary.

The next step is to create and fill a buffer region around each subvolume with particles. The goal of filling this “padding” region with particles is to provide the correct set of nearest neighbors for all the particles in the original, unpadded subvolume, including the particles close to the boundaries. With the correct set of neighbors, all particles in the original, or “local” subvolume will have both their correct density and their correct densest nearest neighbor. The padding is calculated from the average inter-particle spacing in the subvolume. Defining the padding length as  $L_p$ , we calculate the size of the buffer region with

$$L_p = s \sqrt[3]{N_{\text{dens}} V / N}, \quad (1)$$

where  $N$  is the number of particles in the (unpadded) subvolume,  $V$  is the volume of the subvolume, and  $s(> 1)$  is a relative safety factor to account for variations in particle density on the boundaries (see §4.1.4 for a detailed discussion of  $s$ ). The cube-root of  $N_{\text{dens}}$  is included as a multiplier of the mean inter-particle spacing to approximate the distance to the most distant nearest neighbor. In Figure 3,  $L_p$  is shown to be equal on all sides of each subvolume for simplicity, but it is usually advantageous to have different values of  $L_p$  for each face (see §4.1.3). Using communication and a global lookup table of padding values, particles on the boundaries of subvolumes are copied to the appropriate neighbor. In Figure 3, particle  $\alpha_l$ , which is a local particle to subvolume A, has been copied to the padding in subvolume B as  $\alpha_p$ . The situation is reversed for particle  $\beta$ . The particles that reside in the padding constitute the only instance of persistent particle data duplication in this method.

The padding on each face is a function of task count according to periodic boundary conditions. When running in serial, the single task already contains in memory all the particle data required, and padding is unnecessary. At two tasks, only two faces for each subvolume touch a different subvolume, so only two faces need to be padded. Similarly, at four tasks, four faces need padding. Only at eight tasks and above will all six faces of each subvolume require padding.

Once the subvolumes have been appropriately padded, the domain of the halo finding problem has been isolated to only the data present on each task. Each task then independently calculates the densities and nearest neighbors for all of its particles, including the padded particles. With the padding in place, only the fringe padded particles, and none of the local particles, have their density calculated incorrectly.

Each task builds chains of particles similarly to original HOP, but with an additional rule. There may be no chain link created from a padded particle to any type of particle. However, chain links may be made from local particles to any type of particle. This is to

prevent link duplication (any link having to do with a padded particle would otherwise exist in at least one other subvolume), and also false linkages as a result of an incorrect set of nearest neighbors, which only affects padded particles. With sufficient padding, it is a safe assumption that the densest nearest neighbor of a local particle, even if that neighbor is a padded particle, is correct. But there is no such guarantee for a padded particle. This logic is far simpler than an intra-padding distance cutoff, or some kind of nearest neighbor correctness test. This process is depicted in Figure 4, where each task has built several locally-labelled chains. Chains that terminate on the same particle are given the same label, such as  $B_1$ . Allowed links are shown with solid lines, and unallowed “virtual” links are shown with dashed lines.

The next step is an optional, local to each task, premerge of neighboring chains that both have peak densities  $\geq \delta_{\text{peak}}$  (proto-halos) and a boundary density  $\delta_{\text{link}} \geq \delta_{\text{saddle}}$  between them. This step is not in the original HOP method or code. Premerging proto-halos increases the parallelism of the overall chain merging process and reduces the size of the final global boundary density lookup table (discussed below), which reduces the peak memory usage. In some cases, enabling this step can reduce the full runtime by nearly 50%. For every particle in a proto-halo, their  $N_{\text{merge}}$  neighbors are found. If any of the neighbors are in a different proto-halo, the average density of the pair of particles is added to a local lookup table of chain pair boundary densities, if and only if it is the maximum boundary density yet seen for that proto-halo pair. Neighboring particles that are both padded particles are not used when building the lookup table. This rule prevents incorrect proto-halo merging and duplication of relationships. This rule is also followed in the (non-optional) final merging step, described below. When the search is complete, the local lookup table is used to premerge proto-halos.

Because any two proto-haloes that satisfy the above requirements will be merged with or without premerging, these mergers can be done at the local level before the global chain density boundary lookup table is created. The situation is different for sub- $\delta_{\text{peak}}$  chains. Because they merge with only one neighboring chain, the global set of chain relationships needs to be found before they can be merged.

The subdivision of the full volume into subvolumes can result in broken chains if they cross a boundary between subvolumes. To reconstruct the full chains, tasks communicate to their neighbors the chains that terminate on a particle in the padding. Put another way, the “virtual” links are used to identify chains between two tasks that must be joined into a single chain. In Figure 4, Task A communicates to Task B that padded particle  $\beta_p$  is part of chain  $A_2$ . Because Task B has particle  $\beta_l$  in chain  $B_1$ , Task B links the chains  $A_2$  and  $B_1$  together. Chains  $B_2$  and  $A_3$  are similarly linked. The list of linked chains is collected globally, and particles are reassigned to new chains built from these connections. In this fashion, chains

that are broken across boundaries are rebuilt without the requirement of collecting the entire chain particle data on a single task.

Because of the way chains are built and linked across subvolumes, there are particles that are authoritatively assigned to chains on one task, and exist as unassigned padded particles on other tasks. In order to prepare for the final chain merging step, all tasks must be informed of the chain assignments for their padded particles. In this step, each task communicates the chain assignment for its particles that are in the padding of their neighbors. This is based on the set of particles that were communicated earlier to instantiate the padded population, except only the subset of particles with chain assignments need to be communicated this time. For example, in Figure 4 particle  $\alpha_l$  is assigned to the  $A_2+B_1$  chain, and this step assigns particle  $\alpha_p$  on task B to the same chain.

The last part of Parallel HOP builds the final halos out of the separate chains. In this step, both sub- $\delta_{\text{peak}}$  chains and proto-halos are merged using the same logic as in original HOP. Even if proto-halos were previously premerged, this step can merge proto-haloes that have become neighbors after the communication steps above.

As in the premerging step, boundary densities between neighboring chains are added to a local lookup table. The separate lookup tables are globally merged using communication to find the full global collection of chain boundaries that is replicated on all tasks. This global lookup table of chain boundaries can be quite large, especially if premerging is turned off. Using the global lookup table of boundaries, chain merging finishes with precisely the same logic as original HOP, with a few modifications to take advantage of parallelism. The parallelism attempts to split up the work of using the global lookup to make the final halos. However, because the final merging step is a non-local operation, it cannot be distributed using the established domain decomposition, and much of the work ends up unavoidably duplicated.

The result is shown in Figure 5, that groups ( $G_1$  and  $G_2$ ) may have particles in more than one subvolume. The padded particles have been discarded and groups are made up of only the local particles with no duplication.

Once the halos have been identified independently of subvolume, the statistical properties of each halo (dark matter mass, center of mass and maximum radius) are calculated in parallel.

## 4. Parallel HOP Implementation

Our implementation of Parallel HOP is written as part of ‘yt’ (Turk 2008). Yt is an analysis package for AMR data (ENZO in particular) written in the Python programming language. Yt has an array of capabilities that complement Parallel HOP, such as parallel computation of radial halo profiles and volumetric projections. The  $k$ D-tree used by Parallel HOP is KDTree 2 (Kennel 2004), which is written in FORTRAN and is loaded into yt as a module. This is a different and more accurate  $k$ D-tree implementation than the one original HOP uses.

This kind of mixed-code environment exploits the benefits of each language. Python is an object oriented language with very powerful built-in functions and data types. By using a highly-optimized, publicly available FORTRAN  $k$ D-tree, the most computationally costly parts of the calculation can be done using compiled code. This is not to say that Python is slow and inappropriate for large scientific calculations. There are several features and modules of Python that are exploited in Parallel HOP that use optimized and vectorized compiled libraries in the background.

### 4.1. Input and Runtime Parameters

There are a wide variety of parameters that control how Parallel HOP runs. Some are ‘physical’ parameters that directly affect the halos located and have the same function in original HOP and Parallel HOP, others are ‘technical’ that control how Parallel HOP is run, have no analog in original HOP, and in some cases can have a small effect on the halos. Most are user-controlled input parameters, and a few are hard-wired in the source code that are generally not changed. The parameters are described in detail below and are summarized in Table 2.

#### 4.1.1. Parallel HOP Parameters

Of the three density threshold parameters ( $\delta_{\text{outer}}$ ,  $\delta_{\text{saddle}}$ ,  $\delta_{\text{peak}}$ ), only  $\delta_{\text{outer}}$  is a user-controlled setting in Parallel HOP. This is following the recommendation for these parameters given by Eisenstein and Hut, as well as the default settings in the source code of the original HOP implementation. As discussed in the original method paper (see §3, and the tests of the threshold parameters in §2.4), the halos are most sensitive to the value of  $\delta_{\text{outer}}$ , and keeping the other two in a fixed ratio has the advantage of simplifying the operation of the halo finder. Lower values of  $\delta_{\text{outer}}$  increases the number of halos, the total mass in halos and

the mass of the largest halos, and higher values have the opposite effect.

In the original method paper, there are three parameters ( $N_{\text{dens}}$ ,  $N_{\text{merge}}$ ,  $N_{\text{hop}}$ ) that control how many neighboring particles are used for different steps.  $N_{\text{hop}}$  sets how many neighbors are searched over when building chains. In §2.4 of the paper, it is shown that of the three parameters the halos are most sensitive to  $N_{\text{dens}}$ , with higher values reducing the number of small halos. In the original source code, the defaults are for  $N_{\text{hop}}$  to be equal to  $N_{\text{dens}}$  (=65), and  $N_{\text{merge}}$ =4. Because Parallel HOP is designed to best replicate the results of original HOP, these are the settings for Parallel HOP as well.

The  $\delta_{\text{outer}}$ =80.0 line in Figure 6 shows that the default settings of Parallel HOP are a good match for the Tinker et al. (2008)  $\Delta = 300$  halo mass function fitting curve. Also plotted are the  $\delta_{\text{outer}}$ =160.0 and 161.6 mass functions, which shows that as expected, raising the threshold values reduces the number density of halos.

#### 4.1.2. Load-balancing

Parallel HOP in yt employs a sophisticated load-balancing algorithm that allows the use of an arbitrary number of tasks. It is constructed similarly to the simple recursive bisection over particle positions method used in a typical  $k$ D-tree. However, instead of cutting a (sub)volume into only two new subvolumes, this method can cut a (sub)volume into several evenly-populated new subvolumes. The number of cuts in each round, and the total number of cutting rounds, is taken from the prime factorization of the number of tasks. The order of operations is such that the first round of cuts subdivides the full volume into a set of equally-populated subvolumes, where the number of subvolumes is equal to the greatest prime factor. The remaining cuts proceed similarly in descending order of the remaining prime factors, cycling in dimension like a typical  $k$ D-tree. If the number of tasks used is a power of two, this process is identical to a typical  $k$ D-tree construction.

Ideally, the load-balancing would be accomplished by operating on all the particles in the dataset as that would provide the most accurately balanced subvolumes. However, it is unnecessary to operate on the entire dataset. Testing shows that randomly selecting as little as 0.0003% of the full population, and load-balancing on that subset can produce subvolumes with load-imbalances with lower than a 10% spread in terms of particles per subvolume.

Therefore, to load balance a dataset, the first step is to read in a random subset of the particle positions, where the default is a conservative, but still quite small, 3% of all the particles. For maximum efficiency, the data is read off disk in parallel, and communicated to one task, which then load-balances the dataset. The single task then communicates the

boundaries of the derived subvolumes back to all the other tasks, and the analysis moves forward, which includes reading in the full dataset.

Parallel HOP can also be run with load-balancing turned off, in which case the subvolumes are all the same size and shape. With load-balancing turned off, however, the work- and memory-load on tasks can be quite disparate. If the distribution is excessively uneven, there will be tasks with very little workload that are forced to wait on the overloaded tasks, which is very wasteful and inefficient, and runtimes will be high.

#### 4.1.3. *Directional Padding*

The distribution of particles within a subvolume can be highly uneven. In this scenario, the average inter-particle spacing in the subvolume may not be representative of the inter-particle spacing near the faces of the subvolume. In particular, if the particles are sparser near a face than average, the padding distance for that face can be too small to provide enough padded particles for the density kernel. In the opposite case, the padding will be too large and there will be unnecessarily duplicated data.

The solution is to have a different padding value for each of the six faces a subvolume, and to calculate the padding as a function of the inter-particle spacing using just the particles adjacent to that face. Unlike in Figure 3, with this option turned on the padding  $L_p$  will generally not be the same on all sides. This option ensures that each face of a subvolume is given a sufficient amount of padding, no more and no less. In tests, this option has the net effect of reducing the amount of duplicated data without changing the results, and speeding up the overall calculation by five to ten percent.

The particles adjacent to each face used for directional padding are selected as follows. The non-directional padding is found using equation 1 on the entire subvolume. Then, particles that are within that distance from each face are used to re-calculate the inter-particle spacing close to the face, which in turn gives a different padding value for each face. The padding safety parameter  $s$ , described in detail below, is applied to the padding values to get the final, six-faced directional padding values.

#### 4.1.4. *Padding Safety*

It is crucial that all ‘local’ particles in each subvolume have their full and correct set of particles in their smoothing kernel. Because the actual inter-particle spacing can vary over the boundaries of a subvolume compared to the average, the calculated padding must be

increased by some factor to account for low-density pockets. The padding safety parameter  $s$  has a conservative default value of 1.5, but the user can input a different value.

There is not a single correct value of  $s$  because the dynamical range of inter-particle spacing depends on the specific halos and voids present in a dataset. Smaller values are desirable because less padding means fewer particles are copied during communication, and less memory is used on each task. Larger values than what is required have no effect on results, but will slow down the analysis time and uses more memory. On some datasets, values of  $s < 1.5$  will suffice, but on others  $s$  may need to be increased. The default value of  $s$  is large enough for all datasets we have tested, but it is up to the user to ensure it is large enough by varying  $s$  over a range to discover what is sufficient.

To demonstrate the effect of the padding safety parameter on the results, Parallel HOP is run using 8 cores on a dataset with  $128^3$  particles (D128) while varying  $s$ , and compared to the single-core results for which padding is unnecessary (see §5 for details on this dataset). Curves B, C and D in the upper part of Figure 7 show the mean mass change in halos cross-matched from a parallel run to the single-core run. With a small safety factor of 0.01, halos at nearly all mass scales are different, most notably the 40% difference for the largest mass bin. This large difference shows that with a too-small safety factor, the largest halo has been cut nearly in half by the volume subdivision, and not glued back together. Increasing the safety factor to 0.5 shows a dramatic improvement with only a small bump at  $10^7 M_\odot$ , and by  $s = 1.0$  the parallel and single-core halos are identical.

#### 4.1.5. Chain Premerging

The optional premerging step represents a trade-off between consistency and performance. A consequence of premerging is that the halos produced are sensitive to the subdivision of the dataset, and are slightly altered when compared to a non-premerged run. This is because the premerging step is a local operation, and proto-halos close to the subvolume boundary do not have information about nearby proto-halos on adjacent tasks, which alters the eventual make-up of the final halos. It is possible to fix this flaw, but it would require an expensive global communication step prior to premerging, which eliminates the advantages of premerging. This variation only arises when comparing two runs with different settings; running the analysis twice with identical settings gives identical results.

There are three main advantages to premerging. First, because the operation is local to each task, no communication is necessary and work can be done simultaneously on all tasks which increases the overall level of parallelism. Second, it reduces the amount of work

required (sometimes dramatically) in the final, global merging step. Third, premerging can reduce the size of the final chain merging density boundary lookup table, which can be a large data object. Because the global table is replicated on all tasks, the effect of reducing its size is amplified by the number of tasks. On some datasets premerging can reduce the full runtime by a factor of two, and lower the peak memory usage significantly.

A dataset with  $1024^3$  particles (D1024) is used to demonstrate the changes in halos because of premerging (see §5 for details on this dataset). The lower part of Figure 7 quantifies the differences in halos by comparing the mass in halos cross-matched between two runs of Parallel HOP with different settings. Curve E shows that the mean fractional change in halo mass with and without premerging stays below roughly 0.01%. For comparison, curve G shows that a 1% change in  $\delta_{\text{outer}}$  has a much stronger effect on halos than premerging, by roughly two orders of magnitude. The  $\delta_{\text{outer}}=160.0$  and 161.6 lines in Figure 6 show that a 1% change in  $\delta_{\text{outer}}$  results in a virtually indistinguishable difference in the ensemble halo properties. The premerging differences are two orders of magnitude smaller than 1% of  $\delta_{\text{outer}}$ , and therefore premerging is an acceptable trade-off for the sake of performance.

Curve F highlights that the premerging differences are a function of subvolume boundaries. Running with 60 cores produces a different set of subvolume cuts than with 64 cores, which produces a slightly modified set of halos at the same level of variation as in curve E.

#### 4.1.6. *kD-tree Speedup*

The *kD-tree* used here (KDTREE 2) has a feature that makes a resorted internal copy of the particle position data that speeds up the nearest neighbor searches by approximately 17%. This does not translate into a 17% speedup for the entirety of Parallel HOP, but if there is enough memory to contain the duplicated particle data, it is a worthwhile option. It is turned on by default, but the user may turn it off if memory is constrained.

## 4.2. Comparison to Original HOP

This implementation of Parallel HOP can be directly compared to original HOP by running both versions on one processing core on the identical dataset with the same set of parameters. Original HOP is about 40% faster and uses 20% less memory than Parallel HOP. This is because the original HOP *kD-tree* is faster than KDTREE 2, and also from the the additional steps and data objects created as part of the parallel machinery that occur even when run in serial.



Parallel HOP generally does not produce completely identical halos to original HOP. This is because the  $k$ D-tree used in original HOP calculates the distances between particles incorrectly by approximately one part in a million ( $10^6$ ), which affects the smoothing kernel density calculations by up to one part in ten thousand. This difference in distances and densities is enough to make perfect agreement between halos of original HOP and Parallel HOP impossible. Curve A in Figure 7 shows the fractional change in mass in cross-matched halos found by HOP and Parallel HOP on D128. Although the relative errors in smoothing kernel densities are small, the halo masses change by up to 6% in this example. Incorrect distance calculations changes the memberships of the set of nearest neighbors for each particle, modifying the set of neighbors considered when building the initial chains and chain boundary densities. For particles at the centers of halos with densities much greater than  $\delta_{\text{peak}}$  (the densest particles in D128 have  $\delta \approx 5 \times 10^5$ ), a one part in ten thousand change in density is large in absolute terms, and can shuffle the relative peak densities of proto-halos, which can then modify how sub- $\delta_{\text{peak}}$  chains are merged.

### 4.3. Analysis Output

The results of Parallel HOP can be used and output in several ways within yt. The vital statistics (mass, center of mass, etc.) of each halo can be output as a text file. The particle data for each halo can be output into HDF5 files<sup>5</sup>, which allows for detailed post-analysis or visualization of the halos themselves. Halos in yt are represented as data objects that can be immediately passed to other analysis toolkits in yt, such as a halo profiler module, Spectral Energy Distribution (SED) generator (if the simulation contains star particles), or imaging libraries that can make volumetric projections or cutting slices through the halo core.

### 4.4. Modular Portability of Parallel HOP

The core of our implementation of Parallel HOP is written in such a way that porting it to another code base is not difficult. For each task, its input is simply a subset of the particle data and subvolume boundaries, and its output are the halo assignments and kernel densities for the particles, and the halo statistics (center of mass, etc. . .) for all the halos. The core implementation is agnostic to how the data are stored on disk, how it is read into memory, and what will be done with the output. For example, a simple wrapper has been written that reads in raw binary files containing particle data and calls Parallel HOP. We

---

<sup>5</sup><http://www.hdfgroup.org/HDF5/>

encourage inquiries into adapting Parallel HOP for different kinds of datasets.

## 5. Parallel HOP Performance

In this section the results of a suite of benchmarks of Parallel HOP on three ENZO datasets is presented. The smallest dataset contains  $128^3$  dark matter particles in cube  $1 \text{ h}^{-1} \text{ Mpc}$  on a side, the next larger has  $512^3$  particles in a cube  $512 \text{ h}^{-1} \text{ Mpc}$  on a side, and the largest has  $1024^3$  in a cube  $5.6 \text{ h}^{-1} \text{ Mpc}$  on a side. These datasets are referred to as D128, D512 and D1024, respectively. D128 and D512 have been evolved to a redshift of  $z=0$ , and D1024 to  $z=6$ . Parallel HOP is also benchmarked on a fourth dataset with  $2048^3$  particles, but at only one core count, and it is discussed separately in §5.4. All of the benchmarks are run with directional padding turned on.

Except for the largest dataset benchmarked, all of the timings are taken on the Triton Resource<sup>6</sup> at the San Diego Supercomputer Center. The Triton Resource is a high-performance data-intensive machine made up of two clusters of SMP nodes. The Triton Compute Cluster (TCC) contains 256 8-core nodes with 24 GB of shared memory. The Petascale Data Analysis Facility (PDAF) contains 28 32-core nodes, 20 with 256 GB of shared memory and 8 with 512 GB of shared memory. Both clusters have access to the same high-performance disk array and run identical executables. However, a parallel program may use nodes from only one type of cluster at a time, never both simultaneously.

There are some important differences between these datasets and benchmarks. All datasets were analyzed with premerging turned on, and D1024 was also run with premerging turned off. D128 and D1024 are unigrid datasets with 32 and 4096 total grid “tiles” (hereafter simply grids), respectively. D512 is a seven-level AMR dataset with 392,865 grids. There are some extra difficulties associated with AMR datasets with high numbers of grids, such as D512. In ENZO, a particle’s data is stored in the most refined grid that covers the position of that particle. Therefore, a significant fraction, if not all, of the grids in an AMR dataset contain particle data. In the D512 dataset, reading the particle data requires accessing the data from two to three orders of magnitude more grids than the other datasets. This increases the number of disk operations and slows down the reading of data when compared to a dataset with equal numbers of particles that is not AMR (i.e. unigrid). In fact, as shown in Figure 8, at the same core count, reading the particles for D1024 takes roughly the same time as D512, even though D1024 has eight times the number of particles and performs load-balancing.

---

<sup>6</sup><http://tritonresource.sdsc.edu/>

Another difficulty of AMR datasets comes from the startup- and memory-costs associated with building the hierarchy of grids and their spatial relationships in yt. The grid hierarchy is referenced when reading data off disk, and each task must have a full copy of the hierarchy in memory. The grid hierarchy for D512 uses approximately 700 megabytes of memory, which is not insignificant when each task must hold in memory a complete copy.

In datasets of smaller cosmological volumes, the distribution of particles can be highly uneven, while very large volumes are naturally evenly distributed. Therefore, D128 and D1024 are run with load-balancing turned on, and D512 has load-balancing turned off.

## 5.1. Timing Benchmarks

In order to measure the speed of various parts of Parallel HOP, a special command is inserted at various points in the code to record precise time stamps for each task. The locations of the time stamps are chosen to enclose the different functional categories of Parallel HOP in order to carefully gauge how the code scales with respect to core count.

### 5.1.1. Full Timings

In Figure 8 the absolute timing in seconds is shown for each run. The four distinct parts of Parallel HOP are split into subsections of the bars. ‘yt Hierarchy’ refers to the startup costs incurred by the mechanics of yt, which includes reading in the ENZO metadata files and building the grid hierarchy on each task. ‘Reading Data’ covers the time taken to read the particle data off disk and (if selected) the time taken to perform the load-balancing. ‘Parallel HOP’ includes all aspects of Parallel HOP, including the  $k$ D-tree searching, group-building and halo statistics computation. ‘Writing Data’ sums up the time taken to write the halo information to a text file, and one HDF5 file per task containing the particle data for just the halos.

It is clear that the ‘yt Hierarchy’ step is inconsequential to the full timing of Parallel HOP, as it is difficult to discern in any of the runs. This shows that the runtime of this implementation of Parallel HOP is not hindered by the yt framework it relies on.

‘Reading Data’ displays interesting behavior for each of the timings. From one to eight cores on D128, it falls, but rises again through 32 cores. The fall is due to increased parallelism, and the rise is most likely a result of resource competition. The data for D128 is stored in eight separate files, and by 32 cores there are several tasks accessing each file simultaneously. As discussed above, because of the nature of AMR datasets, disk I/O represents

a larger fraction of the full runtime for D512 than the other two, particularly at lower core counts. But the extra challenge of AMR is well parallelized when using more cores; from 2 to 64 cores the time drops by nearly a factor of 20. For D1024 between 8 and 256 cores (also a 32 times increase in core count), the drop is only slightly better than a factor of 4. D1024 exhibits smaller gains because of the extra cost of the initial round of data reading for load-balancing.

The ‘Parallel HOP’ step represents the bulk of the time for most runs, and is discussed in detail below.

Finally, ‘Writing Data’ is indiscernible in most runs and does not impact runtimes significantly. Each task is independently writing data to disk, and the amount of data is much smaller than was read in originally because only the data for particles in halos are recorded as output.

### 5.1.2. *Parallel HOP Timings*

In Figure 9 the parts of Parallel HOP algorithm are examined in detail. Each of the timing blocks plotted is a sum of the maximum time taken by multiple sub-timings in Parallel HOP that fit under the timing block description. A sub-timing contributes time to only one of the timing block categories. Measuring the maximum time in this fashion is more representative of the real computational costs than an average over all tasks because it exposes inefficiencies more clearly. Because Parallel HOP is an asynchronous application, the summed maximum timings includes overlapping processes, which effectively means some time is double-counted. This is why the full sum of the timings in Figure 9 can be longer than the corresponding timing in Figure 8.

‘ $k$ D-tree Searching’ covers the time taken to perform the multiple nearest neighbor searches using KDTree 2. The ‘MPI (+Related)’ step covers both MPI communication activities and operations undertaken by all tasks necessary for parallelism. ‘Halo Creation’ is the time required to perform the merging of chains into final groups. If premerging is turned on, the time taken during that optional operation is included in ‘ $k$ D-tree Searching’ (because searching the  $k$ D-tree constitutes the bulk of the time for premerging). Finally, ‘Halo Statistics’ includes calculation of the halo centers of masses, total masses, maximum radii and bulk velocities.

The timings for the D128 dataset show that it is too small to be efficiently analyzed by Parallel HOP. Between 1 and 32 cores there is very little increase in speed. The MPI overhead starts to dominate the process with task count, and the  $k$ D-tree timings do not

fall quickly enough to compensate for it. This is because at high core counts, the volume of padding needed for each task begins to approach the volume of the subvolumes themselves. This  $k$ D-tree ‘workload floor’ effect is clear when the locations of the linear scaling triangles are compared across all four sets of benchmarks. In all but the D128 timing, the triangles roughly track the top of the  $k$ D-tree timing sections. which shows that the  $k$ D-tree workload scales fairly linearly, except in D128.

The D512 dataset shows much better scaling, except for some odd results in the MPI timings at 4, 16 and 64 cores. A close inspection of the output logs shows that because of the particular distribution of particles, subdividing the full volume without load-balancing turned on at these core counts produces subvolumes that are not as evenly populated as the other core counts. The net effect is that tasks wait on other tasks more, which is reflected in the MPI timings. To a smaller extent it can also be seen in the  $k$ D-tree timings, which don’t fall as fast as might be expected at these particular core counts. Re-benchmarking D512 with load-balancing turned on shows that the MPI overhead is reduced, but the overall runtimes are increased by the extra disk I/O required.

The differences between the two D1024 timings highlights the higher level of parallelism provided by premerging chains. At eight cores, running without premerging is actually faster because there is one fewer nearest neighbor search over the particles. But at higher core counts, without premerging the ‘Halo Creation’ step does not shrink as quickly, and by 256 cores, the premerging run is 25% faster than the run without.

### 5.1.3. *Speedup Plots*

The overall and Parallel HOP-only speedups for each dataset are shown in Figure 10. The Parallel HOP-only line excludes any disk-related operations. At 32 cores, D128 is only 3.1 times faster than a single core run, which shows that Parallel HOP is not appropriate for small datasets. D512 shows much better scaling because it is a larger dataset and therefore more appropriate for Parallel HOP. Again, the odd behavior at 16 and 64 cores can be seen with depressed points at those core counts. The overall speedup for D512 is better than the computational speedup at 64 cores for this same reason, and also because the disk I/O shows very good parallelism between 2 and 64 cores. The advantage of premerging is clear between the two D1024 Figures. At higher core counts the speedup for both premerging curves is significantly higher than the curves without premerging. The gap in the two speedup curves for D1024 is primarily attributable to the cost of load-balancing.

The speedup curves depart from linear scaling for many of the same reasons. Commu-

nication inefficiencies and quantities increase with task count, as does resource competition, which affects D128 and the 256-core D1024 timings the most strongly (see §5.3). The total amount of particles contained in padded regions also rises with core count, which further depresses performance. Variations in the density of particles can have an effect on the load-balancing, both through their bulk distribution as seen in D512 at 16 and 64 cores, and also on the scale of padding, which contributes to load-imbalances between tasks, even when load-balancing is turned on. The workload floor seen in the D128 timings shows that there is a practical ceiling for the number of tasks for a given dataset.

#### 5.1.4. *Weak-Scaling*

Weak-scaling is a good measure of the overhead in a parallel program incurred by the parallel machinery. The problem size and the number of cores used are kept in a constant ratio over a range of core counts, so any increase in total runtime should come from inefficiencies in parallel communication and associated functions. Another motivation for weak-scaling tests is to model the behavior of a code as problem size increases, in terms of both particle and core count. Ideal weak-scaling is flat—the increase in problem size is perfectly compensated for by the commensurate increase in the number of cores.

By randomly subsampling particles from D1024 and analyzing a range of dataset sizes, it is possible to perform a weak-scaling study of Parallel HOP. Because the random subsampling requires modifying the dataset prior to running Parallel HOP, it is impossible read in the data in precisely the same fashion as the other benchmarks. An intermediate step stores the subsampled data on disk, which is read in again for analysis using a different method than the other benchmarks. Therefore, only the timings for the computational parts of Parallel HOP are plotted in Figure 11. The number of particles stored in memory per task is kept constant at roughly  $4.2 \times 10^6$ , but there is some small variability as a result of imperfect load-balancing. The maximum number of particles stored on each task is further increased by 10–20% after padding is considered.

From one core to 256, the computational time required rises from a little over 300 seconds to just under 900. There are a variety of reasons for this rise, but the primary one is that the workload is nonlinear with total particle count. As the total number of particles rises, the sampling of the full dataset’s nonlinear structure improves, and this is reflected in the workload-related statistics over the range of benchmarks. At one core, 8.4% of all particles are in halos, and there are 3,007 initial chains that merge into 1,467 final halos. For 256 cores the figures are 11.4%, 1,170,042, and 124,660, respectively, which averages to 4,570 initial chains per task. The 35% rise in the fraction of particles in halos leads to a 52%

rise in the number of chains per task, and a 389 times increase in the total number of initial chains. Some of this increase is caused by chains broken by the subvolume boundaries (and not entirely due to added structure), which is a function of the number of cores used rather than just particle count.

Each step in Figure 11 is sensitive to these increases. Increasing the fraction of particles in chains means the  $k$ D-tree must perform relatively more nearest neighbor searches for the chain merging steps. The rise in the fraction of particles in chains and halos, and having more chains globally, means more data must be communicated and processed during the MPI steps. More chain interactions via the boundary density lookup table complicates the work of merging chains, which slows down the Halo Creation step. Finally, although the calculation of halo statistical properties is parallelized, and the number of halos rises slower than cores (85 times from one to 256 cores), because halos are global objects, the work cannot be perfectly spread across the cores.

There are some secondary reasons for the rise in runtime. As mentioned in §3.1, between one and eight tasks the number of padded faces for a subvolume rises from zero to six, which in turn increases the workload for the  $k$ D-tree over that range. With the increased number of initial chains, inevitably the load-balance between tasks worsens, leading to increased communication-related inefficiencies, which is reflected in the MPI timings.

Although the rise in runtime is not ideal, weak-scaling can never perfectly flat in practice. Indeed, in light of the nonlinear workload increase, the weak-scaling results are very good. A 256 times increase in total problem size, and all of the nonlinear effects, merely triples the runtime over the base single-core mark.

It is possible to conceive a highly artificial dataset that would reduce the nonlinear effects as follows. Equally-sized clumps of particles evenly gridded in space are placed such that each task contains in memory one clump at the center of its subvolume. No clumps are close to a subvolume boundary, so no chains need reconnecting and padding is unnecessary, nor do any chains merge with chains from a different subvolume. In this scenario, it is expected that the weak-scaling would be much closer to ideal because nearly all the work has been completely localized. However, this is not how datasets are created in practice, and the weak-scaling results presented here are closer to a typical workflow. It is often beneficial to perform low-resolution survey simulations that help tune the settings used for a large and expensive production simulation. When scaling up from the survey simulations to the full size, the behavior of Parallel HOP on the datasets is much closer to the results shown here than an artificial dataset lacking the nonlinear workload increases.

## 5.2. Memory Usage

During the benchmark runs, the memory used for each task is sampled at a number of points during execution, and the peak level recorded. The memory usage for the yt mechanisms separate from Parallel HOP are subtracted, leaving just the memory usage for Parallel HOP. Across all three datasets and core counts there is a nearly universal ratio of peak memory to number of particles (including padding) of 1 megabyte per 4,500 particles. Individual tasks ranged by about  $\pm 20\%$  from this ratio.

At first look, this may appear to be a significant amount memory per particle. It must be noted, however, that the peak memory includes not only the padded particle data, but also the  $k$ D-tree structure, which is significant, as well as the particle chain data (such as particle density and densest nearest neighbor link), and the data objects created for communication. Data sent during communication exists on the sender and receiver simultaneously, briefly duplicating large data objects, and it is during communication steps that peak memory levels are reached.

## 5.3. Cores Per Node

Most of the benchmark runs use multiple cores per node (see Table 1). When using more than one core on a SMP node, the cores compete for access to shared computing resources (such as the memory bandwidth or disk access), and overall runtimes are increased for the individual tasks when compared to single-task timings. In isolated tests for this effect we see that for nearly all the benchmarks there is at worst a roughly 10% slowdown for the most computationally intensive steps due to inter-core competition. However, when running on all 32 cores on a Triton PDAF node, there is a 40% slowdown over a single task which affects the  $k$ D-tree operations most strongly. This only affects the timings of the 256-core D1024 runs, which are the sole case that use all 32 cores on the PDAF nodes.

## 5.4. A Large Dataset

To demonstrate its ability to scale up to larger datasets, Parallel HOP is run on a redshift=0 dataset with  $2048^3$  particles in a cube  $442 \text{ h}^{-1} \text{ Mpc}$  per side. It is run on the Cray XT5 Kraken<sup>7</sup> at the National Institute for Computational Sciences using 350 cores

---

<sup>7</sup><http://www.nics.tennessee.edu/computing-resources/kraken>



on 175 nodes, which collectively provide 2.8 terabytes of memory. The number of nodes is set by the minimum memory requirements needed for the dataset, which are determined by the memory usage scaling factor. Load-balancing, premerging and directional padding are turned on.

The full run takes one hour and two minutes. It spends a negligible amount of time in the ‘yt Hierarchy’ step, 13 minutes in the ‘Reading Data’ step, 41 minutes in ‘Parallel HOP’, and 8 minutes in the ‘Writing Data’ step. It is expected that the scaling performance of this dataset looks something like that of D1024 (with premerging) because load-balancing would have the same effect on the overall performance with core count.

Running Parallel HOP on a dataset this large shows that Parallel HOP is capable of handling very large datasets efficiently. Indeed, no previous public implementation of HOP is at all capable of analyzing a dataset with this many particles. Even if a machine existed that had enough shared memory to contain all the particle data, the run time would be prohibitively long.

## 6. Discussion

We show here that Parallel HOP is a successful parallelization of the HOP algorithm. It can analyze datasets much larger than any previous implementation. It can run on as few as one core, or as many cores as determined by the memory or running time requirements.

Because Parallel HOP is parallelized using domain decomposition, it is particularly well suited for use as an inline halo finder in grid-based cosmological simulation codes. With inline halo finding, galaxy-related objects can be introduced as the simulation runs, such as black holes at the centers of large halos, or galcons (Arieli et al. 2008, 2010), which are a physically-extended analytical model of galactic properties. A detailed merger history can be created for all the halos, which can be used to model the morphologies and star formation histories for the galaxies they contain. Tests of a preliminary inline implementation have shown this to be an effective method for both unigrid and AMR ENZO simulations. The subvolumes on which each task of Parallel HOP runs are identical to that of the simulation, which rules out load-balancing within Parallel HOP as an option. However, because Parallel HOP accesses the particle data directly in memory, it eliminates the sometimes costly ‘Reading Data’ step and speeds up the overall runtime. Additionally, any toolkit available within yt can be applied at the same time to the halos and the entire dataset in general, which enables very powerful and flexible inline analysis.

With regards to the method, the tightest bottlenecks have to do with non-local opera-

tions, such as the ‘Halo Creation’ step. Although the premerging step greatly alleviates that specific problem, it doesn’t fix the root cause of why ‘Halo Creation’ is slow and unparallelized. A true fix would involve a careful modification of how the final halos are created that would remove the global boundary density lookup table, and replace it by many separate lookup tables synthesized from each of the initial local lookup tables.

Future improvements should also include optimization of the code for speed and memory efficiency. Although the most computationally intensive parts of Parallel HOP in yt already use compiled code, replacing some or all of the Python with compiled modules would provide some speedup and memory savings over the current implementation. Hybrid parallelism, in which both MPI and OpenMP are used simultaneously, is an effective way to take advantage of modern multi-core processors. Because Parallel HOP is domain decomposed, hybrid parallelism is a very plausible way to speed up certain parts of the implementation. Replacing the FORTRAN *k*D-tree with an implementation that runs on very fast graphics hardware could provide substantial speed gains on workstations or clusters with that kind of hardware (Zhou et al. 2008).

It is straightforward to adapt the Parallel HOP method, and indeed our implementation as well, for other kinds of cosmological simulational data. Although yt is primarily written with AMR data, because of its modular nature it is possible to write a new data reader within yt to handle other types of particle data. Alternatively, the Parallel HOP implementation source code could be adapted for use inside of a different analysis package fairly easily. Because yt and Parallel HOP are open-source, anyone may freely copy and modify the source code for their own needs.

### 6.1. Parallel HOP and Subhalos

The ability to locate subhalos by using the modifications of HOP in ADAPTAHOP may be a worthwhile feature to add to Parallel HOP. Briefly summarized, ADAPTAHOP finds (sub)halos as follows: Particle densities, and chains of particles (called “leaves” by Aubert et al.), are found identically to HOP. Instead of merging chains and proto-halos by all maximum boundary link values, the “symmetric” boundary densities between chains are found and stored in a lookup table. A “symmetric” boundary means that both chains have links to the other, which is not a requirement in HOP. Subhalos are identified by adjusting a density threshold parameter  $\delta_s$  which is compared to density boundary links ( $\delta_{\text{link}}$  from Fig. 1) between chains. All links  $\delta_{\text{link}} < \delta_s$  are destroyed, which modifies the chain relationships and selects substructure during final merging, which is done very similarly to HOP. For example, if  $\delta_s > (\delta_{\text{AD}}, \delta_{\text{BC}}, \delta_{\text{CD}})$  and  $\delta_s \leq (\delta_{\text{AB}}, \delta_{\text{DE}})$ , chains A and B, and E and D would form two

subhalos. Chain C may be marked as substructure, depending on whether it has particles with density greater than  $\delta_s$ . Finally, subhalos are rejected if their statistical significance falls below the level of Poisson noise.

Because ADAPTAHOP is based on HOP, it should be possible to apply these modifications to Parallel HOP. The modifications would be turned on and off depending on user-controlled parameters. The biggest difference would come from the global chain density boundary lookup table, which would be constructed differently. The modifications would also preclude premerging, as the entire set of density boundary links needs to be preserved for comparison against  $\delta_s$ . The output of Parallel HOP would have to be modified to account for the hierarchies of halos and subhalos, depending on the number of different values of  $\delta_s$  input by the user. The performance of Parallel HOP would be affected by the modifications. The runtime would increase with the number of link threshold parameters  $\delta_s$ . Roughly speaking, the length of the “Halo Creation” step in Fig. 9 would increase linearly. Also, because particles would be multiply-assigned to (sub)halos, and there would be many more (sub)halos, the memory requirements would rise, as would the time of the ‘Halo Statistics’ step.

## Appendix A. Parallel HOP Implementation Source Code

This appendix provides a road-map for understanding our Parallel HOP implementation in detail. The source code is freely available online at the yt homepage<sup>8</sup> as part of the yt distribution. Yt has been built and installed on a wide variety of operating systems, from laptops to supercomputers. It is open-source, and relies on only open-source libraries, so it is free for all to use wherever and however they wish. Yt has an active developer community, and there is a public mailing list linked from the homepage that a user can sign up for to receive assistance on technical issues.

Referring to the numbered glyphs in Figure 2, below is a list that gives the names of source files and functions that accomplish each part of Parallel HOP. Within the yt source, there are three files that contain Parallel HOP functions. They are `yt/lagos/HaloFinding.py`, `yt/lagos/parallelHOP/parallelHOP.py`, and `yt/extensions/kdtree/fKD.f90`, which are referred to as HF, PH and KD, respectively.

1. The command invoked by a user to run Parallel HOP is `parallelHF`, which is contained in HF. It sets default initial values and returns the list of halo objects from Parallel

---

<sup>8</sup><http://yt.enzotools.org/>

HOP at the very end of the analysis. In particular, depending on the user’s settings, the subvolumes are defined in this function (see below), and the padding lengths are calculated, but not filled with particles until later.

2. If load-balancing is set, HF: `_subsample_points` subsamples the particles, and passes the subsampled points to HF: `_recursive_divide` which defines the load-balanced subvolumes.
3. The particle data is read off disk in parallel in HF: `parallelHOPHaloList`. This function then calls the function PH: `_chain_hop`, which is the entry-point function into the halo finding part of Parallel HOP.
4. Using the subvolume boundaries and padding lengths calculated earlier, each task finds its set of neighbors and their padding lengths in PH: `_global_padding` and PH: `_global_bounds_neighbors`.
5. Based on the values of padding for neighboring subvolumes, PH: `_is_inside` marks particles to be communicated to neighbors in PH: `_communicate_padding_data` (and subsequent communication steps), which fills the padding with particles on all tasks.
6. The particle data must be prepared prior to calling the Fortran *k*D-tree in PH: `_init_kd_tree`. This then calls KD: `create_tree` which builds the *k*D-tree and the resorted particle data for search optimization (if set by the user). Next, KD: `chainHOP_tags_dens` is called to calculate the density for all the particles locally on each task, including the padding. PH: `_densestNN` finds the densest nearest neighbor for each particle, which then is used to build the initial chains of particles in PH: `_build_chains` on each task independently.
7. If set, proto-halos are premerged on all tasks independently in PH: `_preconnect_chains`.
8. In order to reconnect chains across subvolume boundaries, the chains must have globally unique identifiers, which is set in PH: `_globally_assign_chainIDs`. Also, because links across boundaries only go ‘uphill’, each task must have a lookup table of the densities of all the initial chains, which is distributed in PH: `_create_global_densest_in_chain`. Once both of those are done, the chains can be reconnected in PH: `_connect_chains_across_tasks`.
9. Prior to the final merging step, padded particles must be assigned to chains authoritatively using communication in function PH: `_communicate_annulus_chainIDs`.
10. The global boundary density lookup table is first built locally on each task in PH: `_connect_chains`, and then merged globally in PH: `_make_global_chain_densest_n`.

11. Processing of the global lookup table happens in PH: `_build_groups`, which defines the final set of particle halos. Using the list of halos, particles are assigned to their halo in PH: `_translate_groupIDs`. Halo total sizes and masses, and centers of masses are calculated in PH: `_precompute_group_info`.

Next, the particle velocities are read in, and the bulk velocity of halos calculated (HF: `parallelHOPHaloList`). The halo objects are created and sorted by halo mass (HF: `_parse_output` and `_join_halolists`). The list of halo objects can then be written to a text file (HF: `write_out`), and the halo particle data stored to HDF5 files (HF: `write_particle_lists`).

This work was partially supported by NSF grants AST-0708960 and AST-0808184. Computations were carried out on the Triton Resource of the San Diego Supercomputer Center and on Kraken at the National Institute for Computational Sciences.

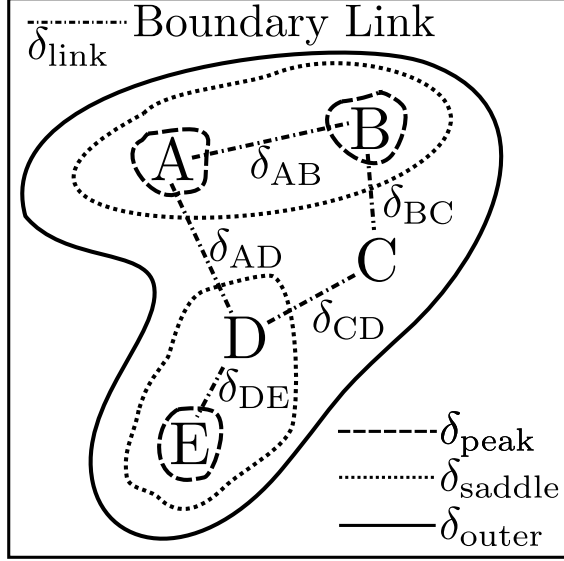


Fig. 1.— Five particle chains are labeled (A through E) at the location of their peak density particle. Density contours surrounding particle chains are shown with lines:  $\delta_{\text{peak}}$  (long-dashed)  $>$   $\delta_{\text{saddle}}$  (short-dashed)  $>$   $\delta_{\text{outer}}$  (solid). The peak of chains A, B, and E lie inside of a  $\delta_{\text{peak}}$  density contour, therefore the chains are considered proto-halos. Spatially proximate chains with neighboring particles are shown linked (dot-dashed lines), and each link has a boundary density  $\delta_{\text{link}}$  value recorded. Proto-halos A and B are merged because their boundary density link lies within a  $\delta_{\text{saddle}}$  density contour ( $\delta_{\text{AB}} \geq \delta_{\text{saddle}}$ ). Although  $\delta_{\text{DE}} \geq \delta_{\text{saddle}}$ , chains D and E do not necessarily merge because D is not a proto-halo. Chains C and D may merge separately or together with proto-halos A, B or E depending on the relative values of the boundary densities  $\delta_{\text{AD}}$ ,  $\delta_{\text{BC}}$ ,  $\delta_{\text{CD}}$  and  $\delta_{\text{DE}}$ .

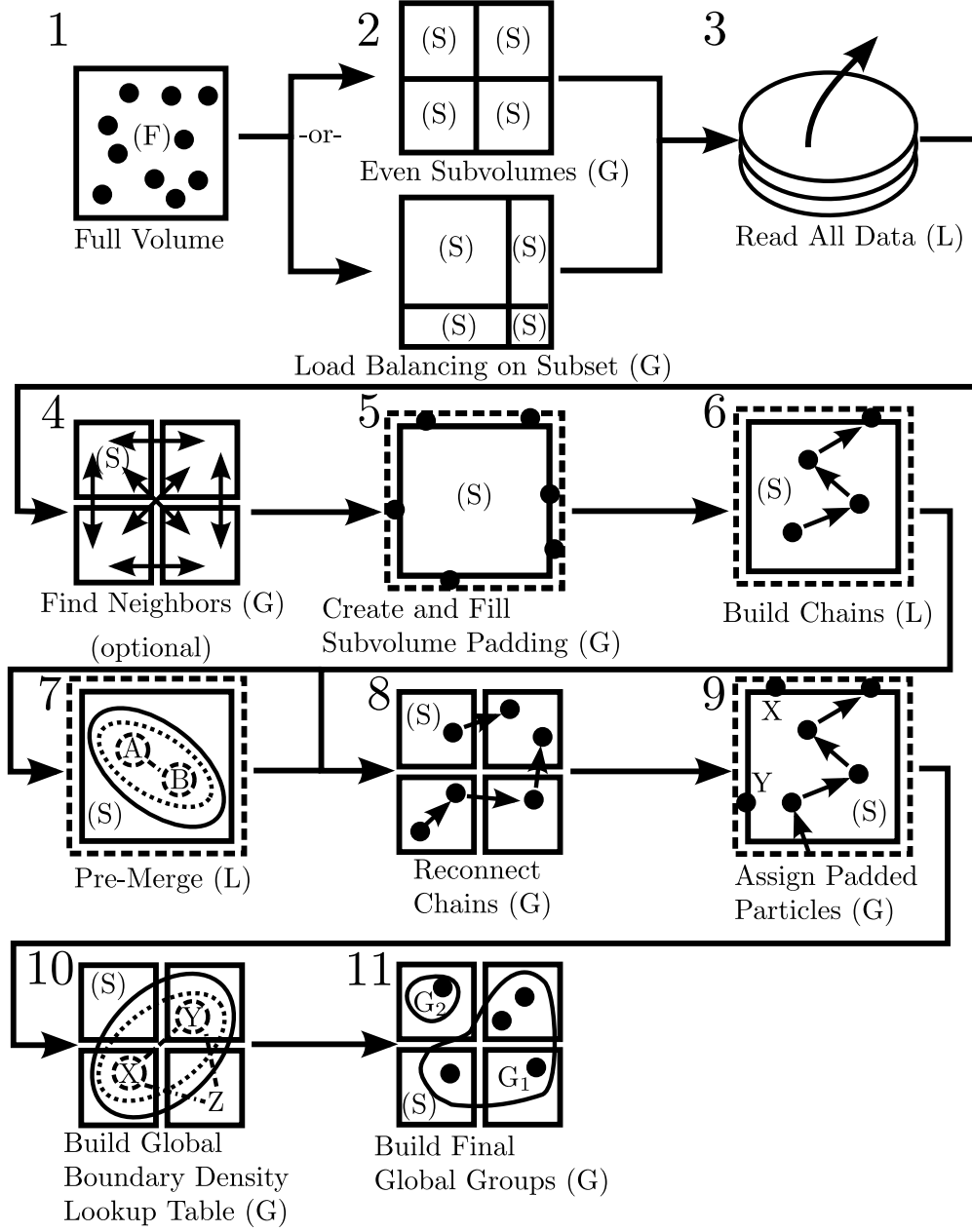


Fig. 2.— Step by step flowchart of Parallel HOP. Inside the boxes (F) and (S) mean the enclosed volume is the full volume or a subvolume, respectively. Chains are labeled with capital letters (e.g. A, B, X), and final groups are labeled by  $G_1$  and  $G_2$ . The letters (G) and (L) following the captions label that step as either a global (using MPI communication) or local operation, respectively. The numbers next to each glyph refer to the steps and code functions described in Appendix A.

Table 1. Cores Per Node

Total Cores	Runs			
	D128	D512	D1024	D1024 (weak-scaling)
	<i>TCC</i> (8 cores/node)	<i>TCC</i>	<i>PDAF</i> (32 cores/node)	<i>PDAF</i>
1	1	...	...	1
2	2	1	...	2
4	4	1	...	4
8	8	2	1	8
16	8	2	2	16
32	8	4	4	32
64	...	8	8	32
128	...	...	16	32
256	...	...	32	32

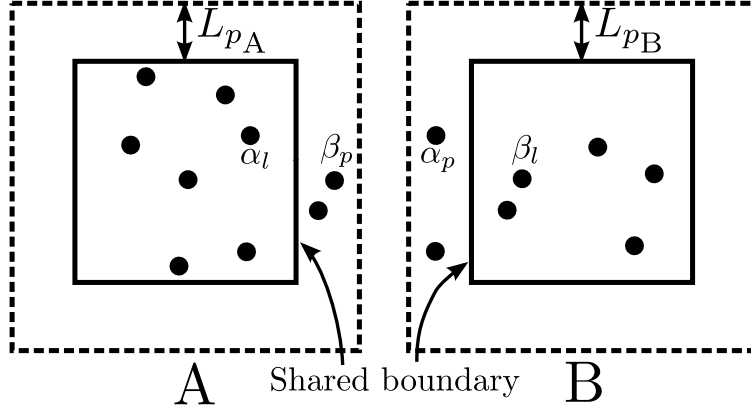


Fig. 3.— Two subvolumes, A and B, are filled with particles inside their initial boundaries (solid lines). A and B share a face-boundary, as shown. Each subvolume is surrounded by padding (dashed lines, padding size  $L_p$ ) in which duplicated, padded particles are placed, that are copied from neighboring subvolumes using MPI communication. Particles  $\alpha_l$  and  $\beta_l$  are the original *local* copies of their *padded* duplicates  $\alpha_p$  and  $\beta_p$ , which are stored in the neighboring padding region. Particles  $\alpha_p$  and  $\beta_p$  are deleted when no longer needed.



Table 2. Parallel HOP Parameters

Parameter	User Controlled?	Default
‘Physical’ Parameters, HOP and Parallel HOP		
$\delta_{\text{outer}}$ : Outer Density Threshold	Yes	80.0
$\delta_{\text{saddle}}$ : Proto-Halo Merging Threshold	No	$2.5\delta_{\text{outer}}$
$\delta_{\text{peak}}$ : Proto-Halo Threshold	No	$3\delta_{\text{outer}}$
$N_{\text{dens}}$ : Smoothing Kernel Size	No	65
$N_{\text{merge}}$ : Chain Boundary Search	No	4
‘Technical’ Parameters, Parallel HOP Only		
Load-balancing	Yes	On
Load-balancing Subsample Fraction	Yes	0.03
Directional Padding	Yes	On
Padding Safety ( $s$ )	Yes	1.5
Chain Premerging	Yes	On
$k$ D-tree Speedup	Yes	On

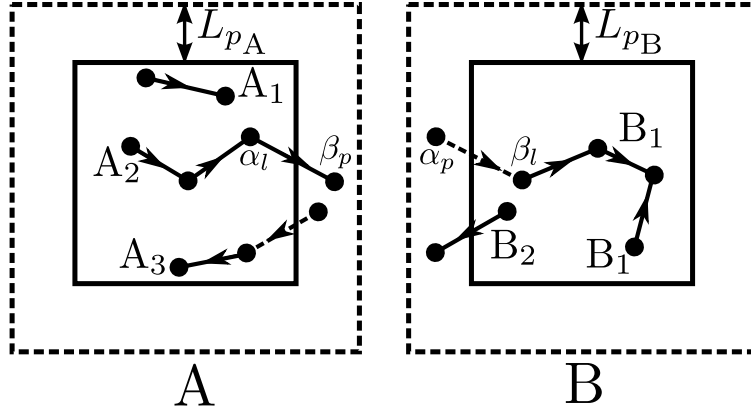


Fig. 4.— Chains of particles are built in each subvolume according to the linking rules (see text). ‘Virtual’ links that are made using communication are shown with dashed lines.

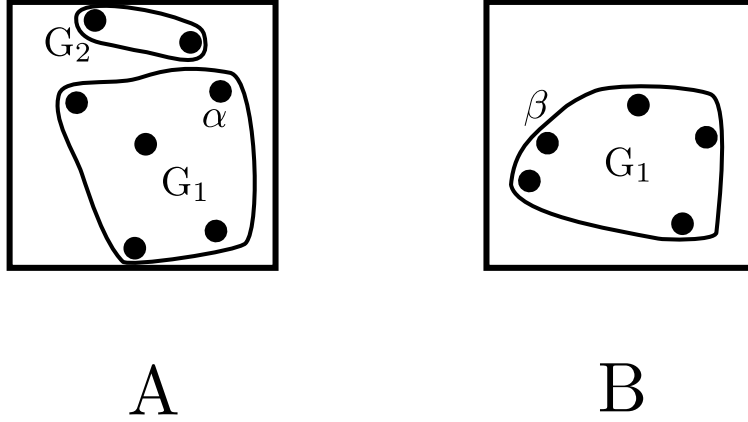


Fig. 5.— Padded particles are removed and groups (or halos) are formed in each subvolume with global labels.  $G_2$  is wholly contained in subvolume A and  $G_1$  has particles in both.

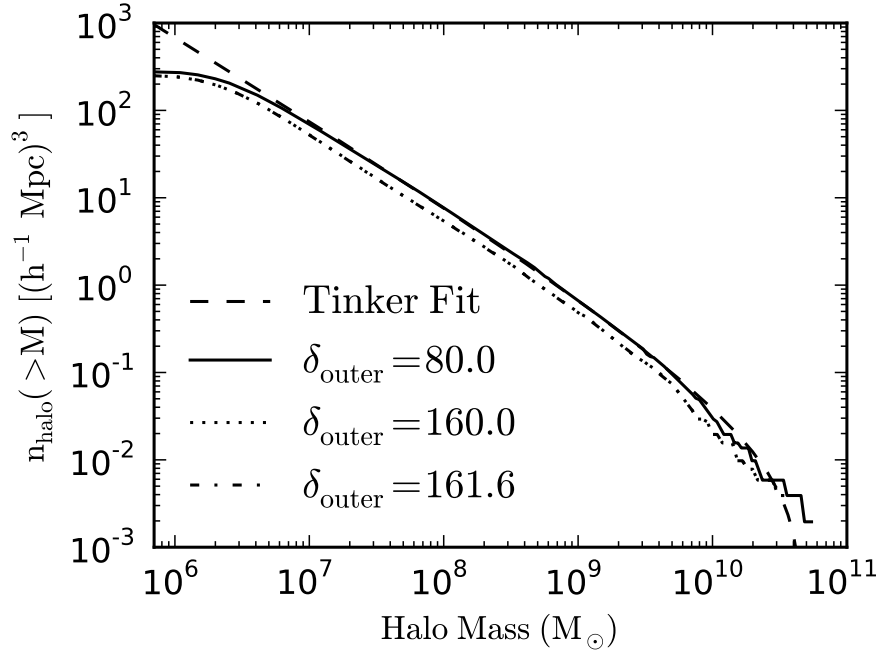


Fig. 6.— The Halo Mass Function for D1024. Three runs of Parallel HOP with default settings and varying the value of  $\delta_{\text{outer}}$ , are plotted in comparison to the Tinker et al. (2008) fit. The  $\delta_{\text{outer}}=80.0$  line very closely matches the  $\Delta = 300$  Tinker fit in the range of  $10^7$ – $10^9$   $M_{\odot}$ . The departure from the fit at the low-mass end is attributable to insufficient mass and spatial resolution, and at the high end from a lack of statistical sampling of massive halos limited by the cosmological volume of the simulation. For comparison, the  $\delta_{\text{outer}}=160.0$  and 161.6 lines are lower in halo number density, and are also indistinguishable from one another.

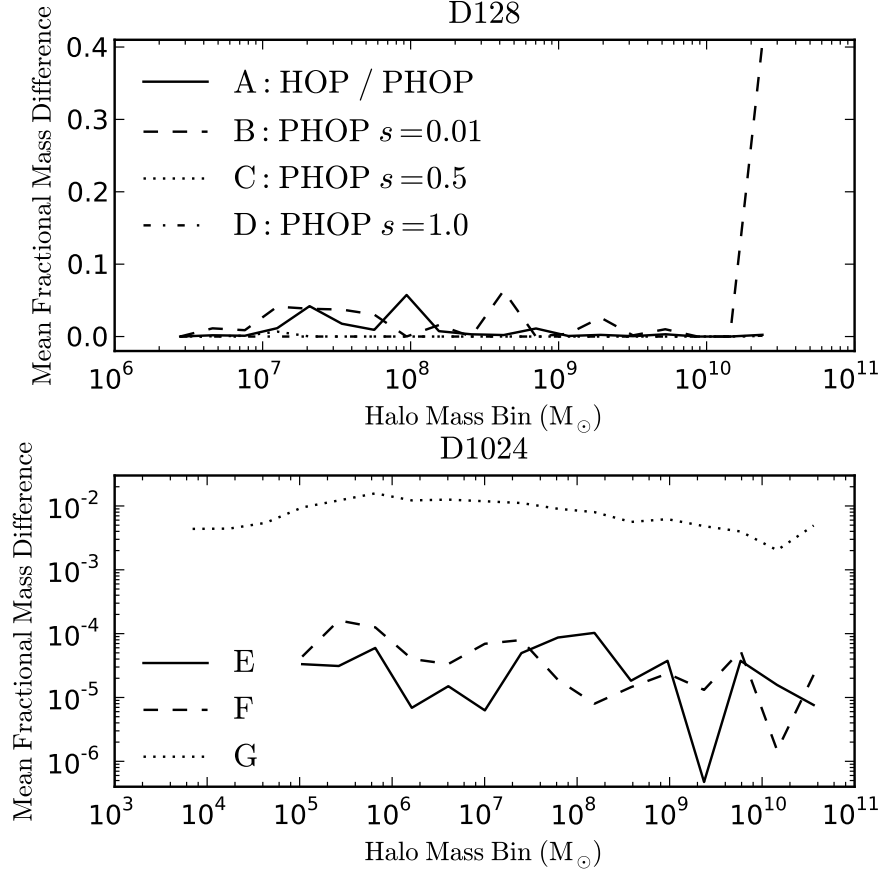


Fig. 7.— The mean absolute fractional change in halo mass in mass bins for cross-matched halos (by center of mass) between runs with different parameters. Fractional differences equal to zero mean the two runs are in agreement. Original HOP and Parallel HOP (PHOP) are run with the default settings (see Table 2) except noted. In the top plot are comparisons using D128, and using D1024 are in the bottom. The parameters varied for comparison are as follows. A: Original HOP compared to PHOP on one core with identical ( $\delta_{\text{outer}}$ ,  $\delta_{\text{saddle}}$ ,  $\delta_{\text{peak}}$ ,  $N_{\text{dens}}$ ,  $N_{\text{merge}}$ ) values. B–D: Single-core PHOP and 8-core PHOP, varying the safety factor  $s$ . E: PHOP on 64 cores with  $\delta_{\text{outer}}=160.0$ , with and without premerging. F: PHOP on 60 and 64 cores with  $\delta_{\text{outer}}=160.0$  and premerging. G: PHOP on 64 cores with premerging, comparing  $\delta_{\text{outer}}=160.0$  and  $161.6$ .

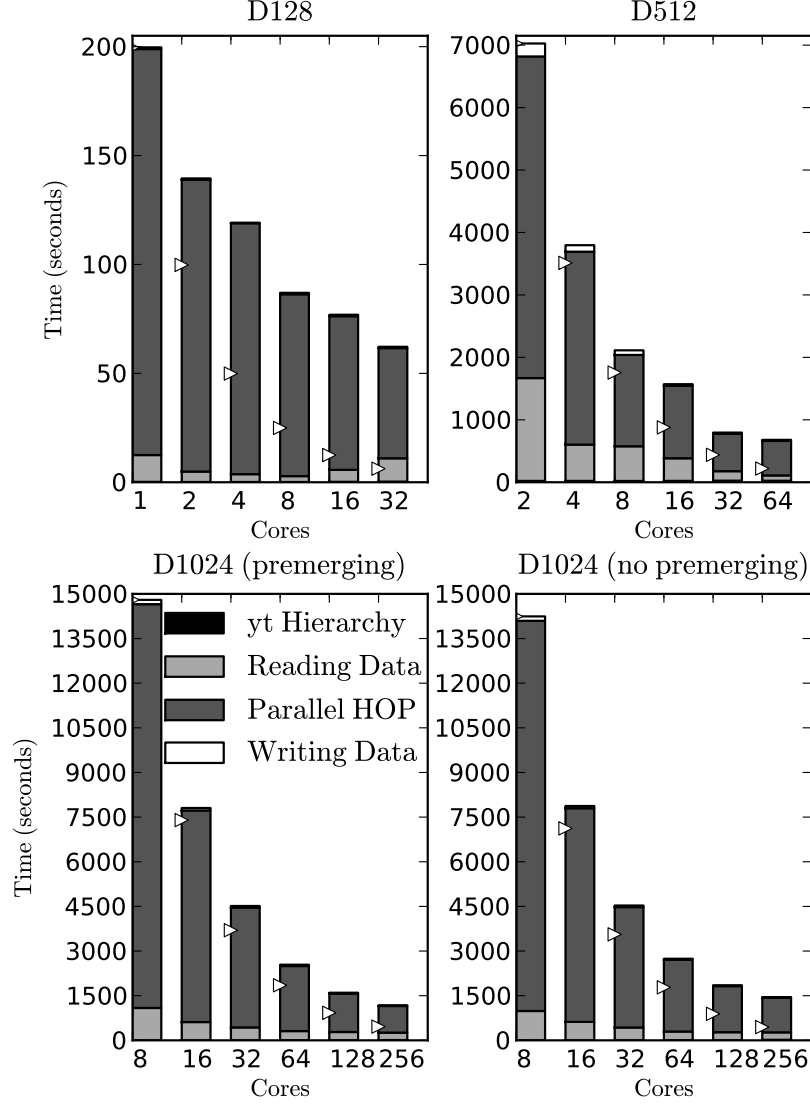


Fig. 8.— Full timings for Parallel HOP on three datasets. Each timing block shows the real-world ‘wallclock’ time taken collectively for all tasks for each step. The triangles show linear scaling based on the smallest core count timing.

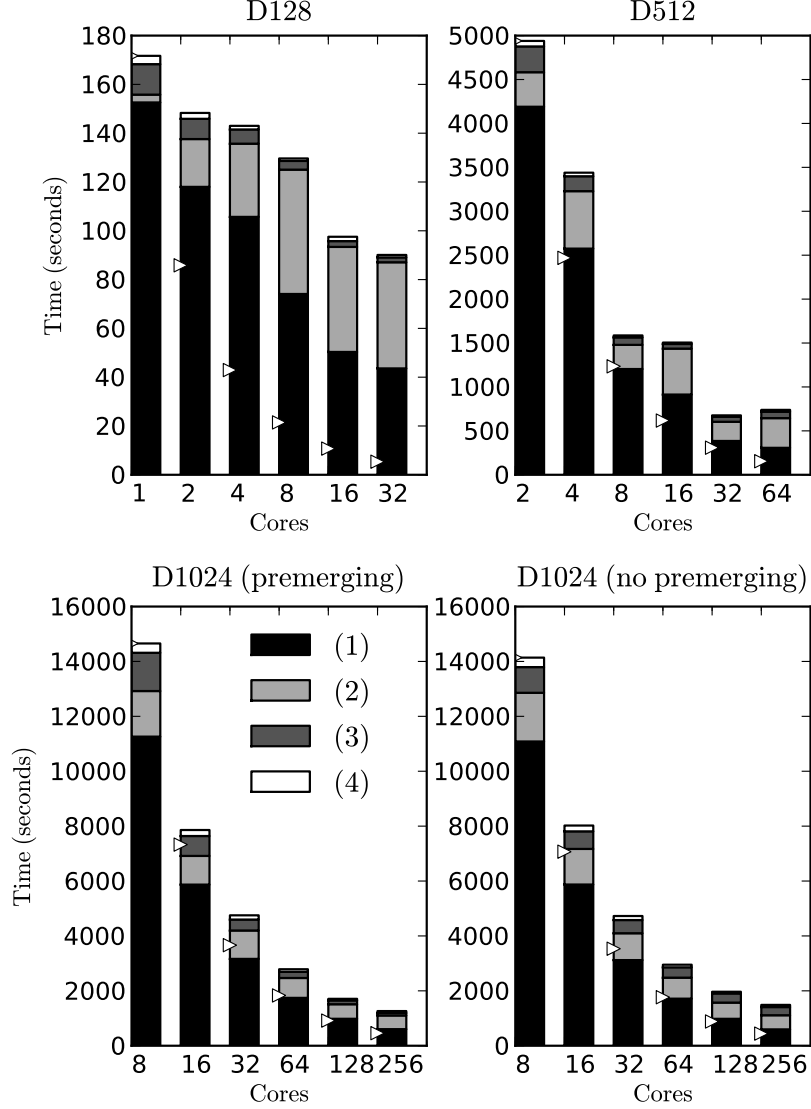


Fig. 9.— Timings for the ‘Parallel HOP’ step. Each timing block is a sum of maximum time taken for several separate steps that are described by the timing block label: (1) -  $k$ D-tree Searching, (2) - MPI and related functions, (3) Halo Creation, and (4) Halo Statistics. The triangles show linear scaling based on the smallest core count timing.

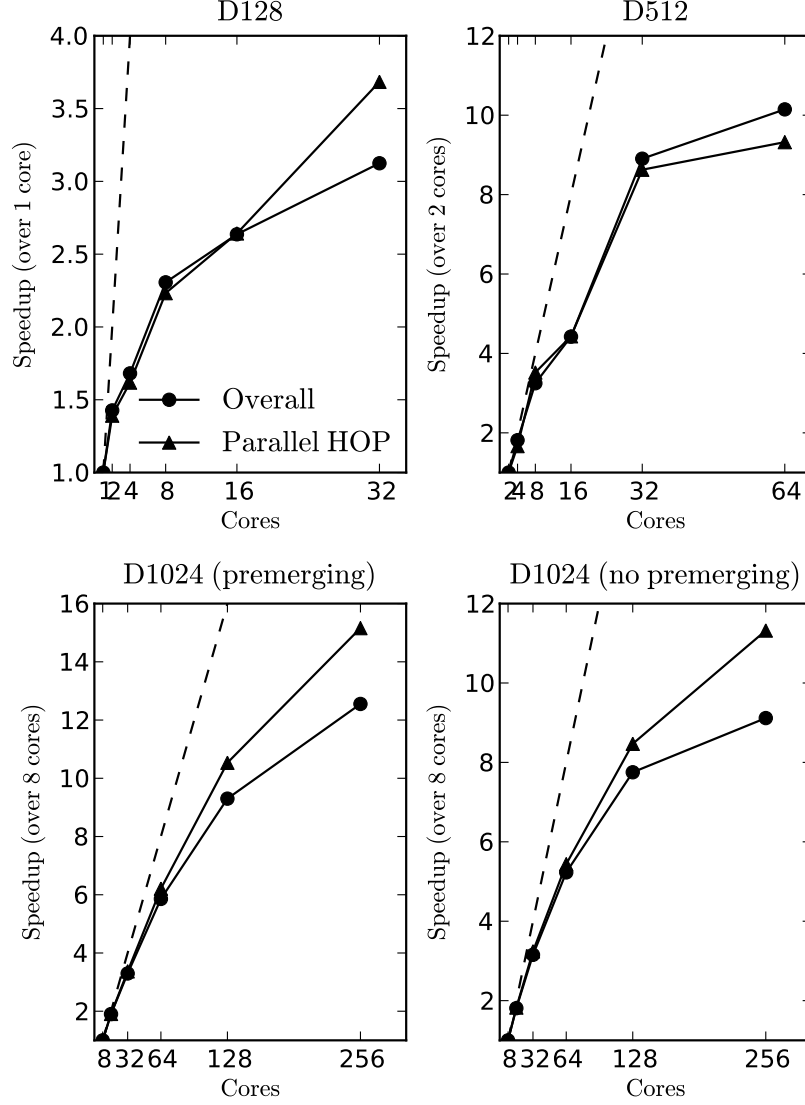


Fig. 10.— Overall and ‘Parallel HOP’ only speedups. Note that the label for 16 cores is missing on the D1024 plots for legibility. The dashed lines show linear scaling based on the smallest core count timing.

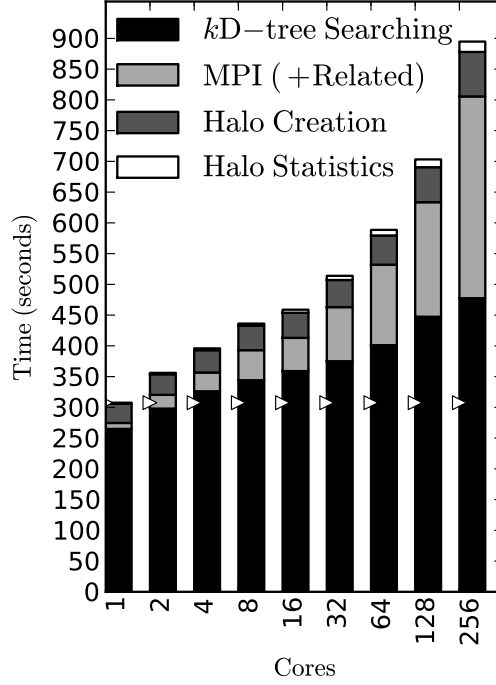


Fig. 11.— Weak-scaling timings on data randomly subsampled from D1024. The size of the dataset analyzed in each run is  $N \times (1024^3/256 = 4,194,304)$ , where  $N$  is the number of cores. The rise in analysis time is a result of a nonlinear increase in workload with particle count. The default settings of Parallel HOP are used for the timings. The triangles show linear scaling based on the single-core timing.

## REFERENCES

- Arieli, Y., Rephaeli, Y., and Norman, M. L.: 2008, *ApJL* **683**, L111
- Arieli, Y., Rephaeli, Y., and Norman, M. L.: 2010, *arXiv:1004.3839*
- Aubert, D., Pichon, C., and Colombi, S.: 2004, *MNRAS* **352**, 376
- Davis, M., Efstathiou, G., Frenk, C. S., and White, S. D. M.: 1985, *ApJ* **292**, 371
- Diemand, J., Kuhlen, M., and Madau, P.: 2006, *ApJ* **649**, 1
- Eisenstein, D. J. and Hut, P.: 1998, *ApJ* **498**, 137
- Friedman, J. H., Bentley, J. L., and Finkel, R. A.: 1977, *ACM Trans. Math. Softw.* **3**, 209
- Gelb, J. M. and Bertschinger, E.: 1994, *ApJ* **436**, 467
- Gill, S., Knebe, A., and Gibson, B.: 2004, *MNRAS* **351**, 399
- Kennel, M. B.: 2004, *arXiv:physics/0408067v2*
- Kim, J. and Park, C.: 2006, *ApJ* **639**, 600
- Klypin, A., Gottlöber, S., Kravtsov, A. V., and Khokhlov, A. M.: 1999, *ApJ* **516**, 530
- Klypin, A. and Holtzman, J.: 1997, *arXiv:astro-ph/9712217*
- Knollmann, S. R. and Knebe, A.: 2009, *ApJS* **182**, 608
- Liu, Y., keng Liao, W., and Choudhary, A.: 2003, in *International Parallel and Distributed Processing Symposium*, p. 82a
- Maciejewski, M., Colombi, S., Springel, V., Alard, C., and Bouchet, F. R.: 2009, *MNRAS* **396**, 1329
- Narayanan, R., Ozisikyilmaz, B., Zambreno, J., Memik, G., and Choudhary, A.: 2006, in *2006 IEEE International Symposium on Workload Characterization*, pp 182–188
- Neyrinck, M. C., Gnedin, N. Y., and Hamilton, A. J. S.: 2005, *MNRAS* **356**, 1222
- Norman, M. L., Bryan, G. L., Harkness, R., Bordner, J., Reynolds, D., O’Shea, B., and Wagner, R.: 2007, *arXiv:0705.1556*
- O’Shea, B. W., Bryan, G., Bordner, J., Norman, M. L., Abel, T., Harkness, R., and Kritsuk, A.: 2004, *arXiv:astro-ph/0403044*



- Pfritznier, D. W., Salmon, J. K., and Sterling, T.: 1997, *Data Mining and Knowledge Discovery* **1**(4), 419
- Shaw, L. D., Weller, J., Ostriker, J. P., and Bode, P.: 2007, *ApJ* **659**, 1082
- Springel, V.: 2005, *MNRAS* **364**, 1105
- Springel, V., White, S. D. M., Tormen, G., and Kauffmann, G.: 2001, *MNRAS* **328**, 726
- Tinker, J., Kravtsov, A. V., Klypin, A., Abazajian, K., Warren, M., Yepes, G., Gottlöber, S., and Holz, D. E.: 2008, *ApJ* **688**, 709
- Turk, M.: 2008, in *Proceedings of the 7th Python in Science Conference*, pp 46–50
- van Kampen, E.: 1995, *MNRAS* **273**, 295
- Voronoi, G.: 1908, *J. Reine Agnew. Math.* **134**, 198
- Weller, J., Ostriker, J. P., Bode, P., and Shaw, L.: 2005, *MNRAS* **364**, 823
- Zambreno, J., Ozisikyilmaz, B., Memik, G., Choudhary, A., and Pisharath, J.: 2006, in *9th Workshop on Computer Architecture Evaluation using Commercial Workloads (CAECW)*
- Zhou, K., Hou, Q., Wang, R., and Guo, B.: 2008, *ACM Trans. Graph.* **27**(5), 1